

RESEARCH ARTICLE SUMMARY

DEVELOPMENTAL BIOLOGY

Reactivation of the pluripotency program precedes formation of the cranial neural crest

Antoine Zalc*, Rahul Sinha*, Gunsagar S. Gulati, Daniel J. Wesche, Patrycja Daszczuk, Tomek Swigit, Irving L. Weissman, Joanna Wysocka†

INTRODUCTION: Cell differentiation is classically described as a unidirectional process that progresses through a series of lineage restriction events, with cellular potential being increasingly reduced as the embryo develops, a concept famously illustrated by Conrad Waddington in his epigenetic landscape. However, the vertebrate-specific transient cell population called cranial neural crest cells (CNCCs) challenges this paradigm. Although they originate in the ectoderm and are capable of differentiating into cell types typical of this germ layer, CNCCs can also give rise to mesenchymal cell types canonically associated with the mesoderm lineage, such as bone, cartilage, and smooth muscle. How CNCCs expand their differentiation potential beyond their germ layer of origin remains unresolved.

RATIONALE: We hypothesized that unbiased analysis of transcriptional heterogeneity during the early stages of mammalian CNCC development may identify a precursor population and provide clues as to how these specialized cells gain their extraordinary differentiation potential. To test this, we combined single-cell RNA-sequencing analysis of murine CNCCs from

staged mouse embryos with follow-up lineage-tracing, loss-of-function, and epigenomic-profiling experiments.

RESULTS: We found that premigratory CNCCs are heterogeneous and carry positional information reflective of their origin in the neuroepithelium, but this early positional information is subsequently erased, with delaminating CNCCs showing a relatively uniform transcriptional signature that later rediversifies as CNCCs undergo first commitment events. We identify an early precursor population that expresses canonical pluripotency transcription factors and gives rise to CNCCs and craniofacial structures. Rather than being maintained from the epiblast, pluripotency factor *Oct4* is transiently reactivated in the prospective CNCCs after head-fold formation, and its expression shifts from the most anterior to the more posterior part of the cranial domain as development progresses. *Oct4* is not required for the induction of CNCCs in the neuroepithelium, but instead is important for the specification and survival of facial mesenchyme, thus directly linking this pluripotency factor with the expansion of CNCC cellular potential. Open chromatin landscapes

of *Oct4*⁺ CNCC precursors are consistent with their neuroepithelial origin while also broadly resembling those of pluripotent epiblast stem cells. In addition, we saw priming of distal regulatory regions at a subset of loci associated with future neural crest migration and mesenchyme formation.

CONCLUSION: Our results show that premigratory CNCCs first form as a heterogeneous population that rapidly changes its transcriptional identity during delamination, resulting in the formation of a transcriptionally (and likely also functionally) equivalent cell group capable of adapting to future locations during and after migration. Such functional equivalency and plasticity of CNCCs is consistent with previous embryological studies. Furthermore, the demonstration that CNCC precursors transiently reactivate pluripotency factors suggests that these cells undergo a natural *in vivo* reprogramming event that allows them to climb uphill on Waddington's epigenetic landscape. Indeed, our results show that at least one of the pluripotency factors, *Oct4*, is required for the expansion of CNCC developmental potential to include formation of facial mesenchyme. Whether this mechanism is specific to CNCCs and if such expansion of cellular plasticity could be harnessed for regenerative medicine purposes remain interesting questions for future investigations. ■

The list of author affiliations is available in the full article online.

*These authors contributed equally to this work.

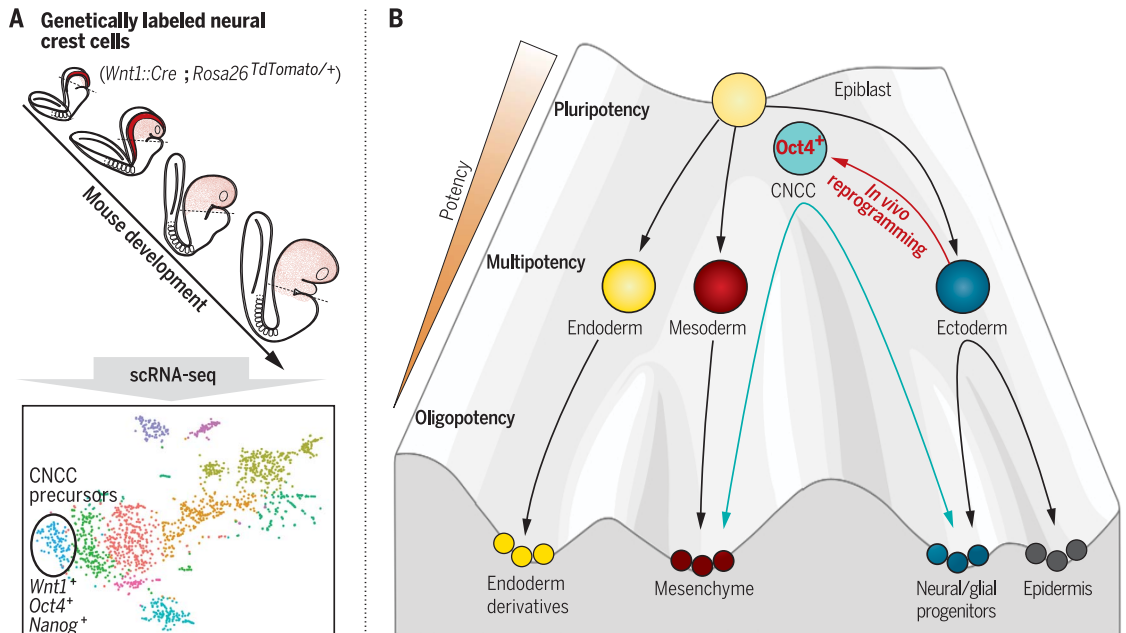
†Corresponding author. Email: wysocka@stanford.edu

Cite this article as: A. Zalc et al., *Science* 371, eabb4776 (2021). DOI: 10.1126/science.abb4776

READ THE FULL ARTICLE AT
<https://doi.org/10.1126/science.abb4776>

CNCCs expand their developmental potential through transient reactivation of a pluripotency program.

(A) Single-cell RNA (scRNA) sequencing of genetically labeled murine CNCCs over 14 hours of development revealed rapid transcriptional changes and identified a precursor population expressing pluripotency factors. (B) Uphill on Waddington's epigenetic landscape, reactivation of *Oct4* endows CNCC precursors with the ability to form derivatives typical of mesoderm, such as mesenchyme.



RESEARCH ARTICLE

DEVELOPMENTAL BIOLOGY

Reactivation of the pluripotency program precedes formation of the cranial neural crest

Antoine Zalc^{1*}, Rahul Sinha^{2*}, Gunsagar S. Gulati², Daniel J. Wesche², Patrycja Daszczuk¹, Tomek Swigut¹, Irving L. Weissman², Joanna Wysocka^{1,2,3,4,†}

During development, cells progress from a pluripotent state to a more restricted fate within a particular germ layer. However, cranial neural crest cells (CNCCs), a transient cell population that generates most of the craniofacial skeleton, have much broader differentiation potential than their ectodermal lineage of origin. Here, we identify a neuroepithelial precursor population characterized by expression of canonical pluripotency transcription factors that gives rise to CNCCs and is essential for craniofacial development. Pluripotency factor *Oct4* is transiently reactivated in CNCCs and is required for the subsequent formation of ectomesenchyme. Furthermore, open chromatin landscapes of *Oct4*⁺ CNCC precursors resemble those of epiblast stem cells, with additional features suggestive of priming for mesenchymal programs. We propose that CNCCs expand their developmental potential through a transient reacquisition of molecular signatures of pluripotency.

Cell differentiation progresses through a continuous lineage restriction process in which cell potential is progressively reduced as the embryo develops. In the early embryo, pluripotent embryonic cells can differentiate into all somatic cell types, but this capacity is rapidly restricted during the formation of the three germ layers, each giving rise to specific and distinct cell types. However, in vertebrates, a stem cell-like population called the neural crest challenges this paradigm. Located at the border between the neural plate and the surface ectoderm, neural crest cells are induced as an epithelial cell type (1, 2) that subsequently undergoes an epithelial-to-mesenchymal transition (EMT), delaminates from the dorsal epithelium, and migrates through the embryo to populate ventral locations, where the population differentiates into diverse cell types (2, 3). Neural crest cells arising from the most rostral part of the embryo, called cranial neural crest cells (CNCCs), not only generate derivatives typical of ectoderm such as neurons and glia but also give rise to cell types canonically associated with the mesoderm lineage, such as bone, cartilage, and smooth muscle (4). Thus, mesenchymal CNCC derivatives, which make up most of the craniofacial skeleton, are often designated as the “ectomesenchyme” to differentiate them from classic mesoderm derivatives

(5). The ability of CNCCs to expand their differentiation potential beyond their germ layer of origin raises the question of whether this pluripotency is induced de novo in the ectoderm or, alternatively, if it is retained from the early pluripotent embryo in a specific subset of neuroepithelial cells. Although the latter scenario has been suggested to be true in *Xenopus* (6), a single-cell transcriptome analysis of *Xenopus* embryogenesis did not find evidence for the maintenance of pluripotency program in developmental trajectories leading to the neural crest (7), leaving the question unresolved. Furthermore, the earliest steps of CNCC formation have not been characterized at the single-cell level in recent transcriptomic studies in mammals (3), and it remains poorly understood how the expanded cell fate potential of CNCCs arises during mammalian embryogenesis.

Transcriptional heterogeneity of early murine CNCCs

We used single-cell RNA-sequencing (scRNA-seq) analysis to characterize the diversity of murine CNCC transcriptomes at four developmental stages from four- to 10-somite stage embryos, corresponding to embryonic day (E) 8 to E8.75 days postcoitum. In the developing head fold, this time span captures CNCC specification in the dorsal neural folds, EMT, migration, and the earliest differentiation decisions. To label CNCCs in the embryo, we took advantage of *Wnt1::Cre*, a well-established premigratory neural crest-specific driver (8). We generated *Wnt1::Cre;Rosa26^{TdTomato/+}* embryos at the aforementioned developmental stages and used flow cytometry to isolate TdTomato⁺ (TdT⁺) cells from their *Hox⁻* cranial portions dissected at the rhombomere 1 level (Fig. 1A and fig. S1A). Because TdT⁺ cells were first

detected at the three- to four-somite stage, we used four-somite stage embryos as the earliest developmental time point for our analysis. We examined single-cell transcriptomes using a modified Smart-seq2 protocol (9), which robustly detected 7000 genes per cell (fig. S1, B and C). On the basis of differential gene expression analysis using Seurat (10), we identified 10 cell clusters with distinct transcriptional profiles (Fig. 1, B and C; fig. S1D; and table S1) falling into two major subpopulations: neuroepithelial precursors, which encompass premigratory CNCCs (clusters 1 to 4 and cluster 10), and migratory mesenchymal CNCCs (clusters 5 to 9) (Fig. 1, B and C, and fig. S1D). Such distinct neuroepithelial and mesenchymal neural crest transcriptional programs have been previously detected in scRNA-seq studies from chick embryos (11, 12). The association of expression signatures with the developmental stage from which each cell originated revealed the following: (i) most cells from the four-somite stage embryos mapped to the neuroepithelial clusters characterized by expression of previously recognized neural crest precursor markers with a primarily neural program (3, 11, 12), such as *Sox2*, *Zic3*, *Otx2*, *Gbx2*, and *Pax2/8*; (ii) the six-somite stage was accompanied by an abrupt transcriptional identity switch, with the emergence of a delaminating CNCC cluster expressing canonical neural crest specification and migration genes such as *Foxd3*, *Sox10*, *Ets1*, and *Twist1*; and (iii) by the eight-somite stage, most cells had transitioned to migratory CNCC clusters and underwent first lineage commitment decisions separating ectomesenchyme from neural and/or glial progenitors (Fig. 1, B and D, and figs. S1D and S2).

Neuroepithelial precursors could be further divided into several transcriptionally distinct subpopulations, characterized by high expression of either *Otx2* or *Gbx2*, but rarely of both (clusters 1 to 3 in Fig. 1, B and C). *Otx2* and *Gbx2* are regionalization markers previously shown to define, respectively, anterior and posterior territories in the developing neural plate, including premigratory CNCCs (13, 14). Given the expression of additional neural plate “positional” genes such as *Rax*, *Hesx1*, and *Dkk1* in *Otx2*⁺ cluster 2 or *En1*, *Hes3*, and *Pax8* in *Gbx2*⁺ cluster 3 (Fig. 1C and figs. S1D, S3, and S4), cells within these clusters correspond to anterior and posterior neuroepithelial precursors, respectively. These precursors encompass premigratory CNCCs with transcriptional signatures reflecting positional information of the surrounding neuroepithelial cells, although they may also contain *Wnt1*⁺ neural progenitors that contribute to the brain (15, 16). However, this positional information is subsequently erased during delamination, because only a single delaminating CNCC cluster was identified (cluster 5 in Fig. 1B). Furthermore, developmental trajectory analysis showed that

¹Department of Chemical and Systems Biology, Stanford University School of Medicine, Stanford, CA 94305, USA.

²Institute for Stem Cell Biology and Regenerative Medicine, Stanford Medicine, Stanford, CA 94305, USA. ³Department of Developmental Biology, Stanford University School of Medicine, Stanford, CA 94305, USA. ⁴Howard Hughes Medical Institute, Stanford University School of Medicine, Stanford, CA 94305, USA.

*These authors contributed equally to this work.

†Corresponding author. Email: wysocka@stanford.edu

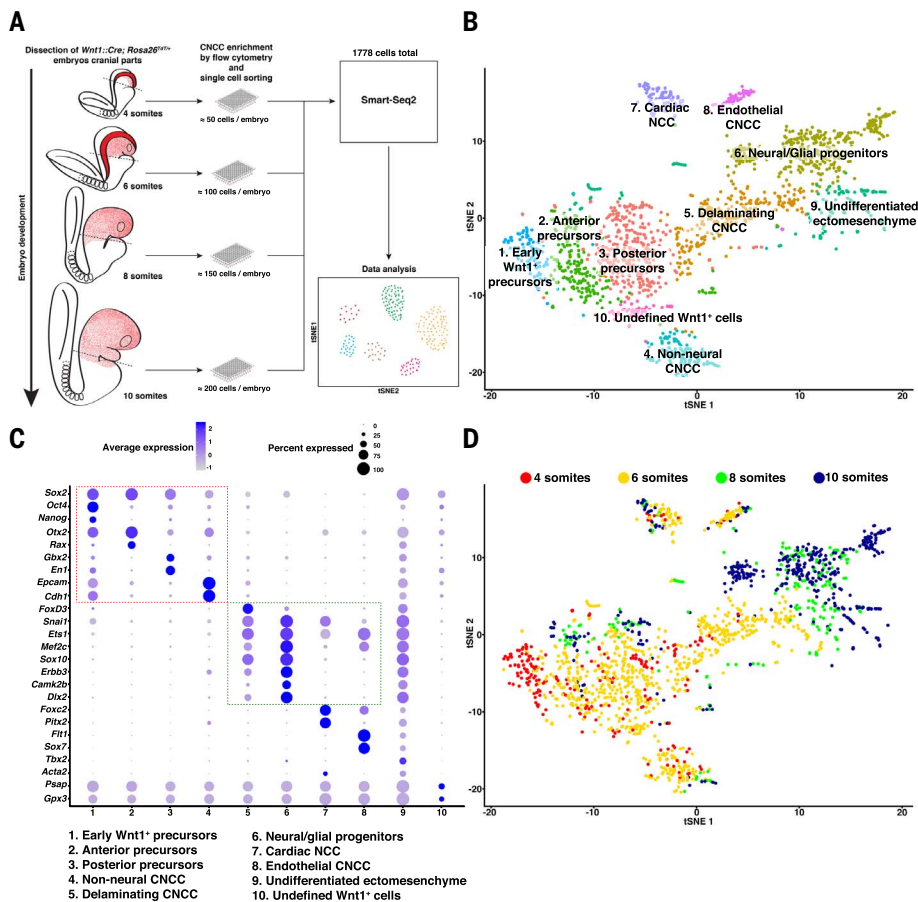


Fig. 1. Characterization of murine CNCC transcriptional heterogeneity with scRNA-seq.

(A) *Wnt1::Cre; Rosa26^{tdTomato/+}* embryos were dissected at the four-, six-, eight-, and 10-somite stages of development at rhombomere 1 level. CNCCs were enriched and single-cell sorted using flow cytometry. scRNA-seq was performed using a modified Smart-Seq2 protocol. (B) t-distributed stochastic neighbor embedding (t-SNE) plot representing all sequenced CNCCs. Cell clusters were obtained based on expressed transcriptome similarities using Seurat. Clusters were annotated based on cluster-specific gene expression calculated by differential gene expression analysis and prior knowledge. (C) Dot plot showing expression of select cluster-enriched genes in CNCC clusters. Dot size indicates percentage of cells expressing listed genes. Blue color intensity indicates average expression level. All genes are within the top 20 most significantly enriched genes for each cluster. Dashed rectangles indicate genes defining premigratory CNCCs (red) or migratory CNCCs (green). (D) Original developmental stage of sequenced CNCCs superimposed on the t-SNE plot shown in (B).

diverse neuroepithelial populations follow a single trajectory of delaminating CNCCs that do not express anterior-posterior (A-P) positional genes and are characterized by a fairly uniform transcriptional signature (Fig. 1C and figs. S1D and S3 to S5). In agreement with previous studies (3), this suggests that although cells are transcriptionally heterogeneous before migration, delaminating CNCCs acquire an equivalent transcriptional program, allowing them to subsequently adapt to environmental cues. After this event, the CNCC population rediversifies as cells undergo lineage decisions and generate their various derivatives.

Early *Wnt1*⁺ precursors dynamically express pluripotency factors

One neuroepithelial precursor population was composed mostly of cells isolated from four-

somite stage embryos and devoid of eight- and 10-somite stage cells (cluster 1 in Fig. 1, B and D, and fig. S2), suggesting that this cluster may represent the earliest *Wnt1*-expressing CNCC precursors (fig. S1D). The canonical pluripotency factors *Oct4*, *Sox2*, *Nanog*, and *Klf4* were all specifically expressed in this cluster, with *Oct4* being among the most highly enriched genes and *Nanog* and *Klf4* expression being almost exclusive to this cluster (Fig. 2A and figs. S4 and S6A). We confirmed *Oct4* and *Nanog* expression in *Wnt1*⁺ cells arising in the dorsal neural folds using RNA fluorescent in situ hybridization (FISH) from *Wnt1::Cre; Rosa26^{tdTomato/+}* four-somite stage embryos (Fig. 2, B and C). We were intrigued by these observations because of the ability of canonical pluripotency factors to reprogram differentiated cells (17) and because these factors were shown

to mark the stem cell niche from which the neural crest arises in avian embryos (12, 18).

We observed that although *Oct4* was most highly expressed in the early *Wnt1*⁺ precursor cluster composed mainly of four-somite stage *Otx2*⁺ cells, by the six-somite stage, *Oct4* expression was down-regulated in anterior precursor cells, whereas it increased in *Wnt1*⁺/*Gbx2*⁺ posterior precursors (fig. S6B). This raised a possibility that *Oct4*⁺/*Wnt1*⁺ double-positive cells first appear in the anteriormost embryo, and then *Oct4* expression shifts posteriorly as development progresses. We used RNA FISH analysis of *Wnt1::Cre; Rosa26^{tdTomato/+}* embryos at the four- and six-somite stages to perform a detailed mapping of *Oct4* and *Nanog* expression along the embryo A-P axis in relation to *Wnt1* expression (i.e., TdTomato) and well-characterized positional markers, such as *Pax6*, *Otx2*, *En1*, and *Gbx2* [Fig. 2, B and C, and figs. S7 to S11 (14)]. We verified that regional markers were enriched within distinct regions along the A-P axis, allowing us to define four domains (figs. S7 to S11). Using this molecular map, we quantified *Oct4* and *Nanog* CNCC expression along the embryo A-P axis and observed strongly reduced expression in the two most anterior domains and increased expression in the most posterior *Gbx2* domain in six-somite stage embryos compared with four-somite stage embryos (Fig. 2, B and C, and figs. S7 to S11). These results support the A-P progression of *Oct4* and *Nanog* expression as the embryo develops.

We further confirmed this A-P shift in expression using *Oct4-GFP* mouse embryos (19), in which we monitored *Oct4* expression through green fluorescent protein (GFP) fluorescence in cranial regions of four- to eight-somite stage embryos. We detected GFP expression in the developing neural folds where prospective CNCCs form, and this expression was lost from the most anterior embryo by the six-somite stage (fig. S12). Taken together, our data suggest that a transient *Oct4*⁺/*Wnt1*⁺ precursor population arises during early CNCC development in the most anterior neural plate and then shifts posteriorly.

Oct4 is reexpressed in prospective CNCCs

To investigate whether *Oct4* is reexpressed in prospective CNCCs or if it is retained from the early pluripotent embryo, we analyzed GFP fluorescence in whole *Oct4-GFP* embryos from E7.5 to the two-somite stage. GFP was detected in the whole epiblast at the early neural plate stage [E7.5; Fig. 2D (20, 21)]. At the head fold stage (late E7.5 and E7.75), GFP was not detected in developing head fold (Fig. 2D; see zoom panel and arrowhead). It was then reexpressed in the most anterior embryo when first somites were forming (Fig. 2D; see arrow), and by the two-somite stage, *Oct4* expression extended posteriorly, whereas the

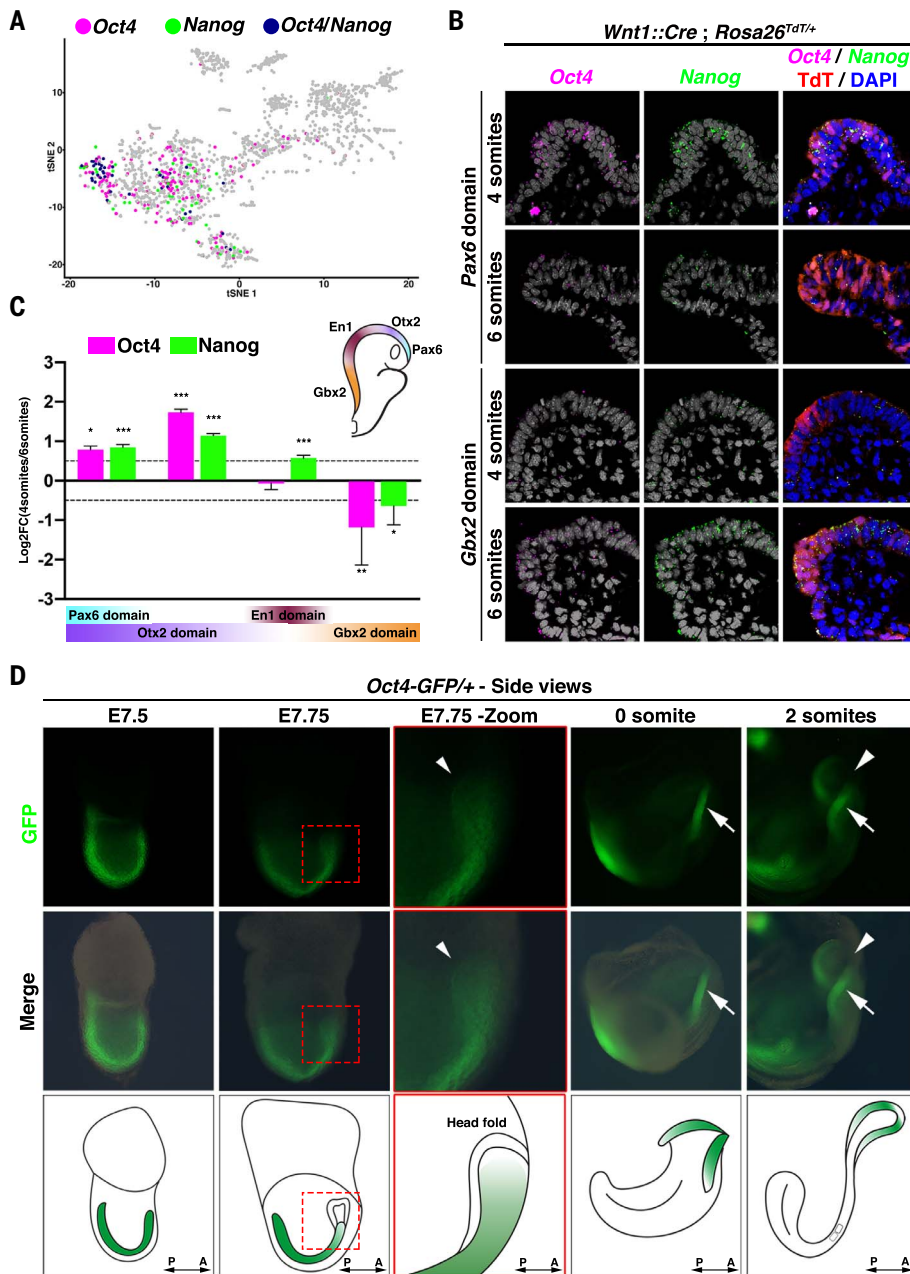


Fig. 2. Premigratory CNCCs transiently induce pluripotency factors. (A) *Oct4* (purple) and *Nanog* (green) expressions were superimposed on the tSNE plot shown in Fig. 1B. *Oct4* and *Nanog* coexpressing cells are indicated in blue. (B) RNA FISH analysis of *Oct4* and *Nanog* expression within transverse cross sections of the most anterior (*Pax6*) and the most posterior (*Gbx2*) cranial domains at the indicated stages of *Wnt1::Cre; Rosa26^{Tdt/+}* embryos. (C) Quantifications of *Oct4* (purple) and *Nanog* (green) expression changes between the four- and six-somite stages along the A-P axis by RNA FISH in *Tdt⁺* cells in dorsal epithelium, as defined by expression of the positional markers *Pax6*, *Otx2*, *En1*, and *Gbx2* (see also figs. S7 to S11). Error bars indicate mean \pm SD. * $P < 0.05$, ** $P < 0.005$, and *** $P < 0.001$ by Mann-Whitney nonparametric statistical test. (D) Side views of *Oct4-GFP/+* embryo cranial regions at the indicated stages. Top panels show the GFP channel, and middle panels show merges between bright-field and GFP channels. Bottom panels are schematic representations of the images above them. A-P orientation is indicated in the bottom right corner. For E7.75 embryos, areas marked with red dashed squares are enlarged and shown in adjacent right panels. Arrowheads show head fold formation without detectable GFP. At the zero-somite stage, arrows mark GFP reexpression in anterior neural folds. At the two-somite stage, arrowheads indicate GFP down-regulation in the most anterior cranial region, and arrows show the GFP expression shift to a more posterior region.

most anterior head fold displayed decreased GFP fluorescence (Fig. 2D; see arrowhead).

To further substantiate that *Oct4* is down-regulated in the rostral neuroectoderm as the embryo transitions from the early (E7.5) to the late (E7.75) neurula stage, we quantified *Oct4* expression in *Sox2⁺* cells along the embryo A-P axis (fig. S13). In the early neurula embryo, the most anterior *Sox2⁺* cells were also expressing *Oct4*. However, in the late neurula epiblast, we consistently found a strong decrease of *Oct4* levels, with the first 10 to 15 anteriormost *Sox2⁺* neuroepithelial cells not expressing *Oct4* (fig. S13). Altogether, these results show that *Oct4* is transiently reexpressed in the prospective CNCC domain at the onset of somitogenesis.

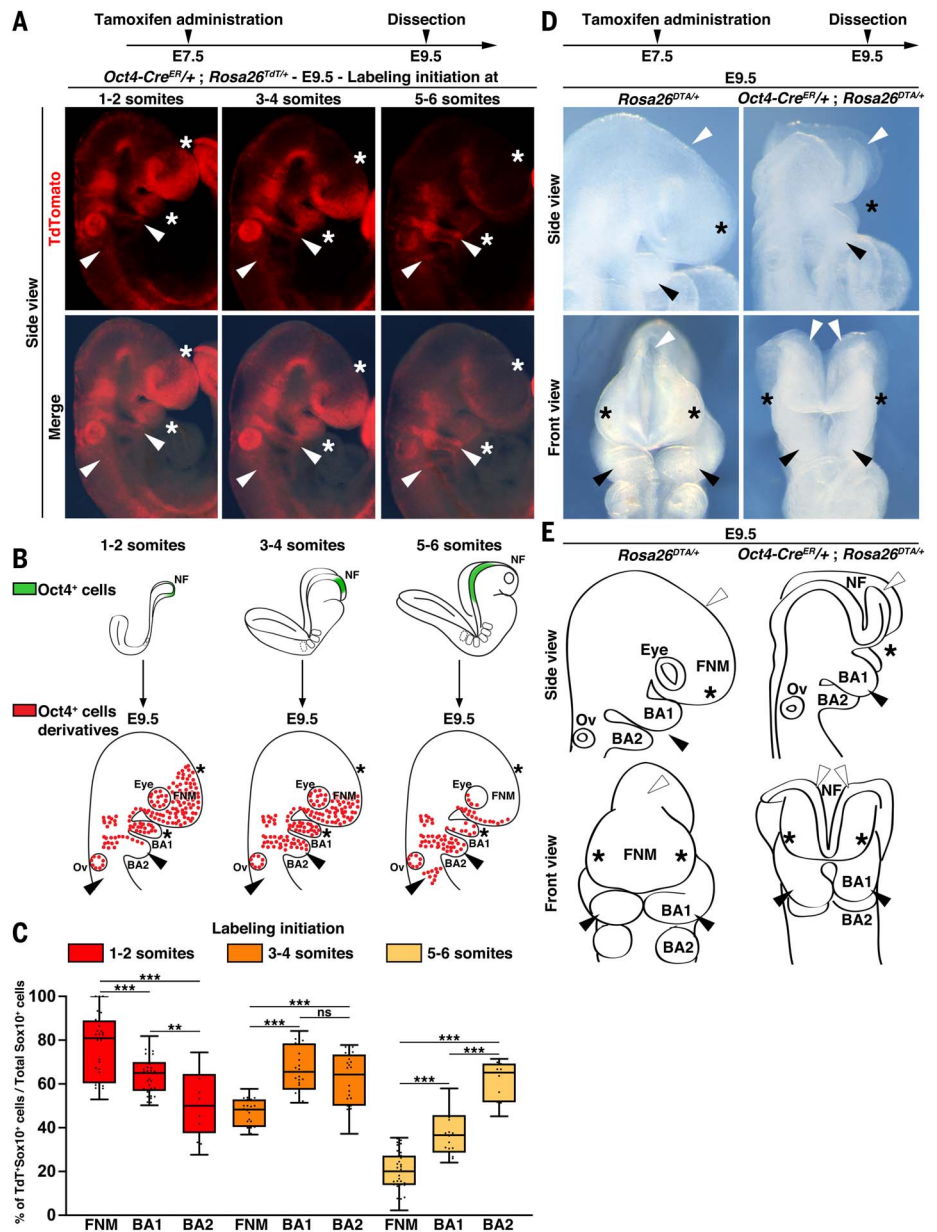
Oct4⁺ precursors give rise to CNCC derivatives

To establish the contribution of the *Oct4⁺* precursors to CNCC derivatives, we generated *Oct4-Cre^{ER/+}; Rosa26^{Tdt/+}* embryos to enable tracking *Tdt⁺* cells at E9.5 before administration of tamoxifen at various earlier stages. Because *Oct4* is expressed throughout the pluripotent preimplantation epiblast [Fig. 2D and fig. S13 (20, 21)], administering tamoxifen at E6.5 resulted in fully labeled embryos (fig. S14A). Therefore, we administered tamoxifen at E7.5. Because *Oct4* expression persists in the trunk through early somitogenesis (22), we inferred the actual onset of cell labeling based on which somites were *Tdt⁻* 48 hours after tamoxifen administration (i.e., at E9.5; fig. S14A). When labeling was initiated at the one- to two-somite stage, *Tdt* strongly labeled the frontonasal mass (FNM) and branchial arch 1 (BA1), confirming that *Oct4⁺* cell descendants generate craniofacial structures. However, when labeling was initiated at later stages, such as at the five- to six-somite stages, *Tdt* was absent from the embryo's most anterior part but was detected in BA1 and BA2 and in streams of cells migrating to form cranial nerve ganglia IX and X (Fig. 3, A and B, and fig. S14, A to C). This A-P shift in *Tdt* labeling dependent on the onset of *Oct4⁺* cells was confirmed by quantifying the ratios of *Sox10⁺/Tdt⁺* double-positive cells to the total number of *Sox10⁺* cells in craniofacial structures of E9.5 embryos (Fig. 3C). Finally, when labeling was induced at late E8.5, *Tdt* was only detected in primordial germ cells (fig. S15), the sole cell type maintaining *Oct4* expression after E9.0 (19, 20), not in more posterior neural crest derivatives, suggesting that *Oct4* reactivation is specific to CNCCs.

If CNCCs arise from transient *Oct4⁺* precursors, then ablation of *Oct4⁺* cells at the onset of CNCC induction should result in the loss of CNCC derivatives. Therefore, we genetically ablated *Oct4⁺* cells upon tamoxifen treatment by using *Oct4-Cre^{ER/+}; Rosa26^{DTA/+}* embryos. We first administered tamoxifen at E7.5 to induce diphtheria toxin (DTA)-mediated

Fig. 3. Cranial *Oct4*⁺ cells are CNCC precursors essential for craniofacial development.

(A) Side views of the cranial region of E9.5 *Oct4-Cre^{ER/+}; Rosa26^{TdT/+}* embryos with time of labeling initiation (in number of somites) indicated. Top panels show the TdTomato (TdT) channel; bottom panels represent merges between bright-field and TdT channels. Asterisks mark TdT expression loss in anterior CNCC derivatives. Arrowheads show TdT expression gain in posterior CNCC derivatives when labeling initiates at later developmental stages. (B) Schematic summary of the lineage-tracking experiments shown in (A). Top panel shows schematic representations of embryo developmental stages at the time of labeling initiation, with *Oct4*⁺ cells marked in green. Bottom panel shows schematic representations of resulting embryos at E9.5, with labeled cells marked in red. Asterisks mark craniofacial structures progressively losing TdT expression. Arrowheads indicate prominences gradually gaining TdT expression BA, branchial arch; Ov, otic vesicle. (C) Quantifications of Sox10⁺/TdT⁺ assessed by immunofluorescence within transverse cross sections of the indicated craniofacial prominences of E9.5 *Oct4-Cre^{ER/+}; Rosa26^{TdT/+}* embryos, with timing of labeling initiation (in number of somites) indicated. Error bars indicate mean ± SD. ***P* < 0.01 and ****P* < 0.001 by Mann-Whitney nonparametric statistical test; ns, nonsignificant. (D) Side and front views of E9.5 *Rosa26^{DTA/+}* and *Oct4-Cre^{ER/+}; Rosa26^{DTA/+}* embryos treated with tamoxifen at E7.5. Asterisks indicate missing frontonasal mass (FNM) in *Oct4-Cre^{ER/+}; Rosa26^{DTA/+}* embryos. Black and white arrowheads point to BA1 and the neural folds (NF), respectively. (E) Schematic representations of embryos shown in (D). Asterisks indicate missing FNM in *Oct4-Cre^{ER/+}; Rosa26^{DTA/+}* embryos. Black and white arrowheads point to BA1 and the NF, respectively.



Oct4⁺ cell ablation between E7.5 and E8.0, corresponding to the onset of CNCC formation, but after *Oct4* requirement in postimplantation epiblast and germ layer specification (23, 24). Resulting mutant embryos analyzed at E9.5 displayed a complete absence of FNM (Fig. 3, D and E). Neural folds were present, indicating that the observed craniofacial phenotype was not a secondary effect of a massive failure in the neural plate and/or fold formation and confirming that cranial *Oct4*⁺ cell population is selectively required for CNCC development. This phenotype resembled that of *Wnt1::Cre; Rosa26^{DTA/+}* embryos (fig. S16). Both phenotypes were similar to those previously reported in avian embryos that underwent cranial neural crest ablation (25). When we induced *Oct4*⁺ cell ablation at E8.5, mutant

embryos presented with virtually normal frontonasal processes and cephalic vesicles; however, nasal processes were absent (fig. S17), which is consistent with the A-P shift in *Oct4* expression. Altogether, these results show that *Oct4*⁺ cells define a transient CNCC precursor population that is first induced anteriorly and then shifts posteriorly and gives rise to craniofacial structures.

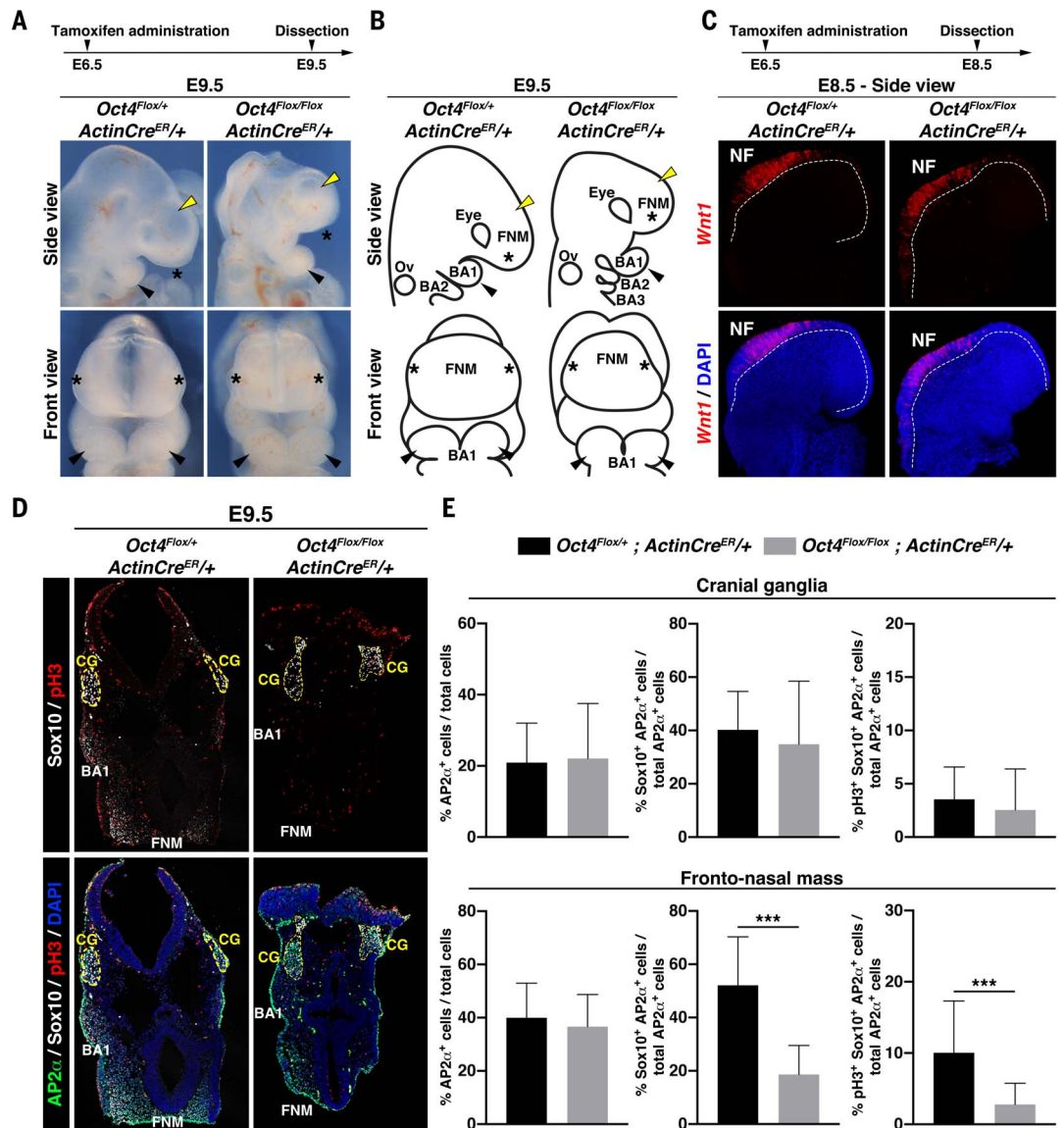
Oct4 is required for proper ectomesenchyme specification, proliferation, and survival

To assess whether *Oct4* is necessary for CNCC formation, we generated *Oct4^{Flox/Flox}; ActinCre^{ER/+}* mutant embryos to perturb *Oct4* function. About 24 hours are needed for *Oct4* mRNA levels to be significantly reduced after *Oct4* locus recombination (24). Thus, we administered

tamoxifen at E6.5 to ablate *Oct4* expression after gastrulation but before *Wnt1* up-regulation (26) and neural crest induction. Resulting *Oct4* mutant embryos presented with severely reduced facial prominences (Fig. 4, A and B, and fig. S18, A and B). However, RNA FISH against *Wnt1* revealed similar expression in controls and *Oct4* mutant embryos, showing that *Oct4* is not required for *Wnt1* induction in the neuroepithelium (Fig. 4C and fig. S18C). Further, immunostaining against the neural crest markers AP2α (Fig. 4, D and E) and Alx4 (fig. S18, D to G) demonstrated that although facial prominences were reduced in mutant embryos compared with controls, similar proportions of the remaining cells expressed AP2α and Alx4 (Fig. 4E and fig. S18, E and G), consistent with *Oct4* marking early CNCC

Fig. 4. *Oct4* is dispensable for CNCC induction but essential for ectomesenchyme specification.

(A) Side and front views of E9.5 *Oct4^{Flox/+};ActinCre^{ER/+}* and *Oct4^{Flox/Flox};ActinCre^{ER/+}* embryos treated with tamoxifen at E6.5. Asterisks indicate reduced frontonasal mass (FNM) in *Oct4^{Flox/Flox};ActinCre^{ER/+}* embryos. Black and yellow arrowheads point to branchial arch 1 (BA1) and the cephalic vesicle, respectively. **(B)** Schematic representations of embryos shown in (D). Asterisks indicate reduced FNM in *Oct4^{Flox/Flox};ActinCre^{ER/+}* embryos. Black and yellow arrowheads point to BA1 and the cephalic vesicle, respectively. **(C)** Side views of whole-mount RNA FISH against *Wnt1* performed on E8.5 *Oct4^{Flox/+};ActinCre^{ER/+}* and *Oct4^{Flox/Flox};ActinCre^{ER/+}* embryos treated with tamoxifen at E6.5. Images are maximum projections. Dashed line indicates the neural folds (NF) limit. **(D)** Immunofluorescence against AP2 α , pH3, and Sox10 within transverse cross sections of E9.5 *Oct4^{Flox/+};ActinCre^{ER/+}* and *Oct4^{Flox/Flox};ActinCre^{ER/+}* embryos treated with tamoxifen at E6.5. Cranial ganglia (CG) are indicated by yellow dashed lines. **(E)** Quantification of proportions of AP2 α cells, Sox10⁺/AP2 α cells, and pH3⁺/Sox10⁺/AP2 α cells in CG (top) and FNM (bottom). Error bars indicate mean \pm SD. ****P* < 0.001 by Mann-Whitney nonparametric statistical test.



precursors but being dispensable for CNCC induction and delamination.

By contrast, within CNCC derivatives, we observed a strong reduction in the proportions of Sox9⁺/Alx4⁺ and Sox10⁺/AP2 α ⁺ cells in facial prominences of E9.5 *Oct4* mutant embryos compared with controls. This was accompanied by an 80% reduction in the proportion of pH3⁺ cycling CNCCs and a 10-fold increase in the levels of cleaved Caspase3⁺ apoptotic CNCCs, which together likely account for the observed decrease in size of facial prominences (Fig. 4, D and E, and fig. S18, D to G). However, the development of neural and/or glial CNCC derivatives such as cranial ganglia, which also receive contributions from the *Oct4*⁺ precursors (fig. S14, B and C), appeared unaffected by *Oct4* loss, as evidenced by the lack of effects on Sox10 expression and proliferation in these derivatives (Fig. 4, D and E). In aggregate, these data are consistent with the model in which

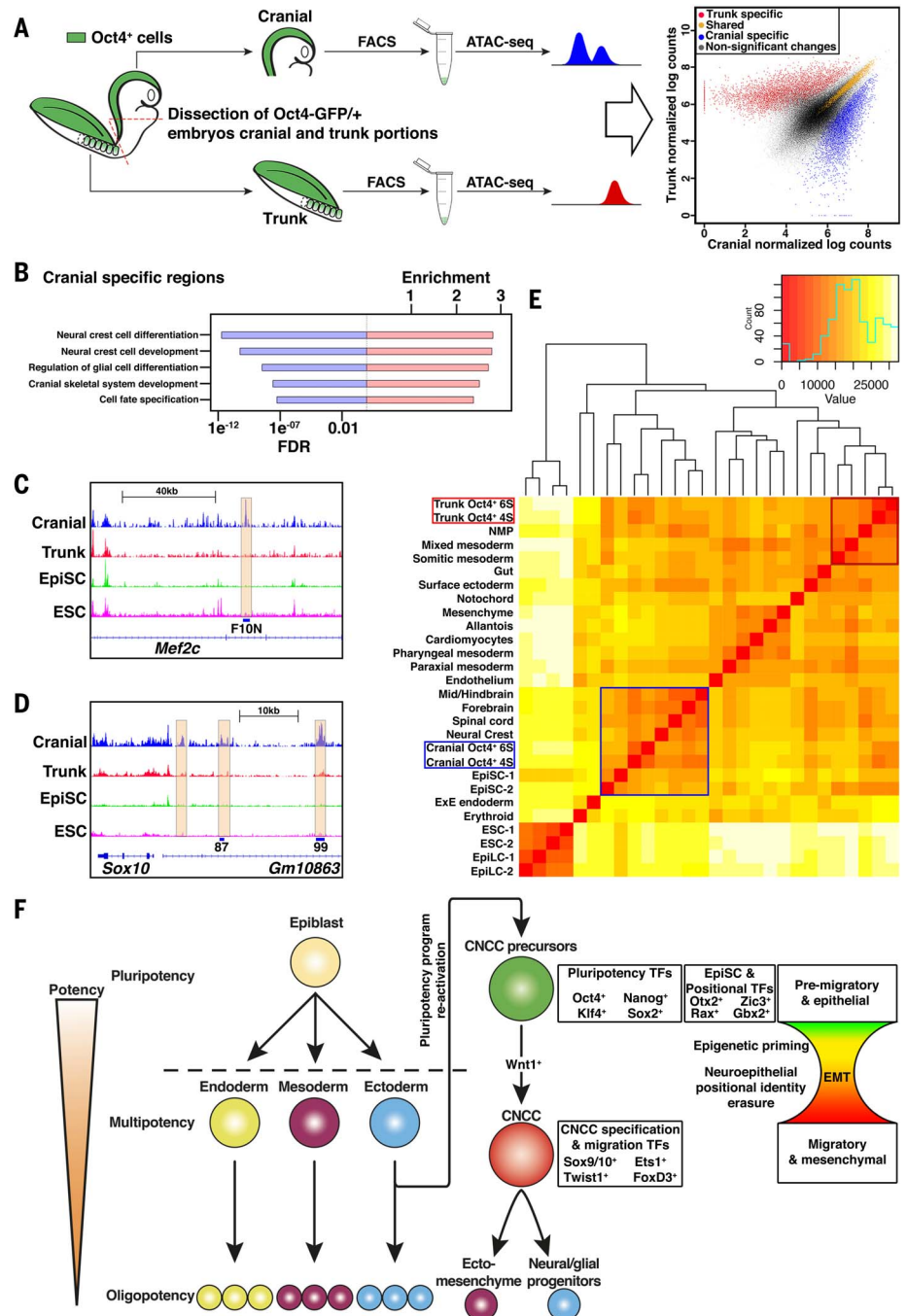
Oct4 marks the early CNCC precursor population but is not required for entry into the neural crest program. Instead, it is essential for ectomesenchyme specification and survival, directly linking this pluripotency factor to the expansion of developmental potency in the neural crest.

Ectomesenchyme priming of *Oct4*⁺ premigratory CNCC regulatory programs

To gain insights into open chromatin landscape and cis-regulatory features of *Oct4*⁺ CNCCs, we performed ATAC-seq (assay for transposase-accessible chromatin using sequencing) analysis of *Oct4*⁺ cells isolated from the cranial region of *Oct4-GFP/+* four- to six-somite stage embryos (Fig. 5A). During early somitogenesis, in the posterior trunk of the embryo, *Oct4* expression is maintained from the postimplantation epiblast, through the posterior primitive streak, to multipotent neu-

romesodermal progenitors (22, 24, 27). To enable stage-matched comparisons of hypersensitivity patterns, we sorted trunk *Oct4*⁺ cells from the same embryos. We compared ATAC-seq patterns of cranial and trunk *Oct4*⁺ cell populations focusing on promoter-distal peaks, most of which correspond to enhancers. We defined cranial-specific (blue) and trunk-specific (red) ATAC-seq peaks (Fig. 5A) and analyzed the underlying transcription factor (TF) sequence motifs. Cranial-specific ATAC-seq peaks were enriched in motifs for the Otx2, Sox, Zic, and Ap2 TF families, which are known to be expressed in the neuroepithelium during CNCC induction and specification [table S2 (2)]. By contrast, trunk-specific regions were almost exclusively enriched in various homeobox motifs, as might be expected given that at least a subset of trunk *Oct4*⁺ cells were undergoing axial specification when isolated [table S3 (28, 29)].

Fig. 5. Regulatory landscape of cranial Oct4⁺ cells showing similarity to EpiSCs and epigenetic priming for migratory fates. (A) *Oct4-GFP/+* embryos were dissected at the four- and six-somite stage to assess chromatin accessibility in cranial (dissected at the rhombomere 1 level) and trunk (dissected at the first somite level) Oct4⁺ cells using ATAC-seq. ATAC-seq enrichments at distal regulatory regions are shown, with cranial-specific Oct4⁺ cells in blue, trunk-specific Oct4⁺ cells in red, and shared regions in orange. (B) Gene ontology using GREAT showing the five most enriched biological processes associated with cranial-specific promoter-distal hypersensitive regions. (C and D) Genome browser tracks representing ATAC-seq signals in the vicinity of *Mef2c* (C) and *Sox10* (D) in mouse ESCs, EpiSCs, and cranial and trunk Oct4⁺ cells. In (C), the shaded box indicates cranial Oct4⁺ cell-specific accessible region overlapping with the *Mef2c*-F10N enhancer active in migrating CNCCs (31). In (D), the shaded boxes indicate cranial Oct4⁺ cell-specific open regions, two out of three overlapping regions orthologous with previously characterized enhancers (87 and 99) active in migratory avian CNCCs (12). (E) Clustering analysis of ATAC-seq data from cranial and trunk Oct4⁺ cells together with ESCs, EpiSCs (34), and EpiSCs (33) and all major cell types present in E8.25 mouse embryo from an atlas of single cell ATAC-seq (32) represented as a heatmap. Red square indicates tissue clustering with trunk Oct4⁺ cells. Blue square highlights cell types clustering with cranial Oct4⁺ cells. (F) Model representing CNCC formation through a transient precursor state expressing canonical pluripotency factors and primed for the acquisition of mesenchymal potential.



We next performed gene ontology analysis using the GREAT annotation tool (30). We found that top enrichment categories at trunk-specific regions included pattern specification, regionalization, and limb development (fig. S19A), whereas top ontology enrichments for cranial-specific Oct4⁺ regions were all related to the neural crest and its derivatives and included neural crest cell development and differentiation, regulation of glial cell differentiation, and cranial skeletal system development (Fig. 5B). Loci driving these associations included genes such as *Sox10*, *Mef2c*, *Pdgfra*, and

Twist1, which are poorly expressed in Oct4⁺ CNCCs, but are induced later, in delaminating and migrating CNCCs (fig. S19, B to D). Examination of ATAC-seq signals at these loci confirmed the presence of cranial-specific accessible regions in their vicinity in the absence of detectable expression of the genes in early CNCC precursors (Fig. 5, C and D, and fig. S19E). We detected a cranial-specific open chromatin region within the *Mef2c* gene corresponding to previously characterized *Mef2c*-F10N enhancer active in migrating CNCCs [Fig. 5C (31)]. Similarly, at the *Sox10* locus, we identified three

cranial-specific accessible regions (Fig. 5D), two of which with orthologous sequences that have already been characterized in migrating CNCCs of avian embryos (12).

These observations suggest that the Oct4⁺ CNCC cis-regulatory landscape is primed for future activation of migration and differentiation programs. To systematically characterize the relationship between cranial Oct4⁺ cell-specific ATAC-seq peaks from the four- to six-somite stage embryos and gene expression, we linked these peaks to their closest genes and analyzed expression of the associated gene set

in our scRNA-seq data at different developmental stages. This revealed the highest enrichments of the associated genes among those expressed at the 10-somite stage (fig. S19F), consistent with priming of distal cis-regulatory regions before expression of their target genes.

Similarity between the cis-regulatory landscapes of cranial Oct4⁺ precursors and epiblast stem cells

We compared ATAC-seq patterns of cranial and trunk Oct4⁺ cells with a wide set of cell types at a similar stage of development, E8.25 (32), and also included data from three well-characterized Oct4⁺ pluripotent cell states: mouse embryonic stem cells (ESCs), epiblast-like cells (EpiLCs), and epiblast stem cells (EpiSCs) (33, 34). Clustering analysis revealed that (i) trunk Oct4⁺ cells cluster with somitic mesoderm and neuromesodermal progenitors; (ii) cranial Oct4⁺ cells cluster with EpiSCs and, consistent with their neuroepithelial origin, with mid/hindbrain, forebrain, and neural crest; and (iii) both cranial and trunk Oct4⁺ cells cluster away from other pluripotent cell types such as ESCs and EpiLCs. These results are consistent with the predicted developmental relationships of cranial and trunk Oct4⁺ cells and uncover the similarities of the open chromatin landscapes of cranial Oct4⁺ and EpiSCs (Fig. 5E). Indeed, 66% of distal ATAC-seq peaks from EpiSCs are also hypersensitive in cranial Oct4⁺ cells (fig. S20A). Furthermore, ATAC-seq peaks shared between EpiSCs and cranial Oct4⁺ cells were enriched for categories associated with transcriptional regulation and development, in contrast to ATAC-seq peaks, which are specific to EpiSCs (fig. S20, B and C). These observations suggest that mammalian CNCCs transiently reacquire developmental regulatory programs similar to those of pluripotent EpiSCs.

Discussion

Through unbiased analysis of single-cell transcriptomes over 14 hours of early murine CNCC development, we uncovered highly spatiotemporally dynamic and diverse molecular identities of this specific cell group. Our data show that upon formation, premigratory CNCCs carry A-P information reflective of their neuroepithelial origin, as has been described in central nervous system regionalization (35). However, in contrast to the latter system, positional identity is erased during delamination as migratory CNCCs lose expression of neuroepithelial positional genes and adopt a more uniform transcriptional signature. We speculate that this erasure generates a functionally equivalent CNCC population that can readily adapt to future migratory and postmigratory locations. Such a model would explain previously documented adaptation of premigratory CNCCs

to a new position upon transplantation at a different axial level (36) and is consistent with widespread Polycomb-dependent bivalent chromatin marking at promoters of facial patterning genes in early CNCCs, followed by the resolution of bivalency into transcriptionally active states in response to environmental cues (37).

Our work identified a transient precursor population that expresses both canonical pluripotency transcription factors and neuroepithelial markers, gives rise to CNCCs, and is essential for the formation of craniofacial structures. Oct4 not only marks CNCC precursors but is also required for proper ectomesenchyme specification and survival, directly linking the function of this pluripotency factor with an expansion of CNCC developmental potential. Furthermore, recent work in *Xenopus* suggests that the homeodomain protein Ventx, a frog homolog of Nanog, is also required for ectomesenchymal potential of CNCCs (38). These observations raise the conundrum of how transcription factors expressed in neuroepithelial precursors affect downstream ectomesenchyme development (one possibility is through priming of distal regulatory regions). Such priming of developmental enhancers before activation of their target genes has now been observed in a variety of biological systems (11, 12, 37, 39, 40).

We also found that open chromatin patterns of Oct4⁺ CNCC precursors broadly resembled those of EpiSCs. Although EpiSCs are pluripotent, their transcriptional features are reminiscent of the early primitive streak (41). Furthermore, we noted that both CNCC precursors and EpiSCs express not only pluripotency factors but also *Zic3* and *Otx2*, two factors that set up EpiSC enhancer landscapes (42, 43). These similarities in transcription factor repertoire likely account, at least in part, for similarities in cis-regulatory programs. Thus, CNCC precursor molecular signatures are reflective of both transient reactivation of pluripotency and priming toward future neural crest fates (Fig. 5F).

Materials and methods summary

For scRNA-seq, cells were isolated as single cells from dissected cranial portions of *Wnt1::Cre; Rosa26^{tdTomato}* embryos using flow cytometry. Developmental stages were inferred based on the number of somite pairs. Single sorted cells were processed using a modified Smart-Seq2 protocol (9), and data were analyzed using Seurat. For ATAC-seq, cells were sorted as described above and processed following the ATAC-seq protocol described previously (44). Libraries were prepared following Illumina protocols and sequenced using the NextSeq 500 system (Illumina).

Embryos were imaged using a Leica M165 FC stereoscope coupled with fluorescence

when needed. Immunostaining was done using classical procedures. FISH was performed following manufacturer guidelines (ViewRNA Cell Plus Assay, catalog no. 88-19000-99, Thermo Fisher Scientific). Probes were designed by Thermo Fisher Scientific. Whole-mount FISH was performed following HCR version 3.0 instructions for whole-mount staining (Molecular Instruments). The *Wnt1* probe was designed by Molecular Instruments. Samples were imaged using a Zeiss LSM 800 confocal microscope. Images were stitched together and processed with Photoshop software (Adobe Systems).

Image quantifications were performed using Cell Profiler version 3.0 (45). Error bars were calculated as mean \pm SD using a Mann-Whitney nonparametric statistical test; **P* < 0.05, ***P* < 0.01, and ****P* < 0.001. At least three embryos were analyzed for each genotype and each developmental time point.

REFERENCES AND NOTES

1. E. Theveneau, R. Mayor, Neural crest migration: Interplay between chemorepellents, chemoattractants, contact inhibition, epithelial-mesenchymal transition, and collective cell migration. *Wiley Interdiscip. Rev. Dev. Biol.* **1**, 435–445 (2012). doi: [10.1002/wdev.28](https://doi.org/10.1002/wdev.28); pmid: [23801492](https://pubmed.ncbi.nlm.nih.gov/23801492/)
2. M. Simões-Costa, M. E. Bronner. Establishing neural crest identity: A gene regulatory recipe. *Development* **142**, 242–257 (2015). doi: [10.1242/dev.105445](https://doi.org/10.1242/dev.105445); pmid: [25564621](https://pubmed.ncbi.nlm.nih.gov/25564621/)
3. R. Soldatov *et al.*, Spatiotemporal structure of cell fate decisions in murine neural crest. *Science* **364**, eaas9536 (2019). doi: [10.1126/science.aas9536](https://doi.org/10.1126/science.aas9536); pmid: [31171666](https://pubmed.ncbi.nlm.nih.gov/31171666/)
4. N. M. Le Douarin, S. Creuzet, G. Couly, E. Dupin. Neural crest cell plasticity and its limits. *Development* **131**, 4637–4650 (2004). doi: [10.1242/dev.01350](https://doi.org/10.1242/dev.01350); pmid: [15358668](https://pubmed.ncbi.nlm.nih.gov/15358668/)
5. J. A. Weston *et al.*, Neural crest and the origin of ectomesenchyme: Neural fold heterogeneity suggests an alternative hypothesis. *Dev. Dyn.* **229**, 118–130 (2004). doi: [10.1002/dvdy.10478](https://doi.org/10.1002/dvdy.10478); pmid: [14699583](https://pubmed.ncbi.nlm.nih.gov/14699583/)
6. E. Buitrago-Delgado, K. Nordin, A. Rao, L. Geary, C. LaBonne. Shared regulatory programs suggest retention of blastula-stage potential in neural crest cells. *Science* **348**, 1332–1335 (2015). doi: [10.1126/science.aaa3655](https://doi.org/10.1126/science.aaa3655); pmid: [25931449](https://pubmed.ncbi.nlm.nih.gov/25931449/)
7. J. A. Briggs *et al.*, The dynamics of gene expression in vertebrate embryogenesis at single-cell resolution. *Science* **360**, eaar5780 (2018). doi: [10.1126/science.aar5780](https://doi.org/10.1126/science.aar5780); pmid: [29700227](https://pubmed.ncbi.nlm.nih.gov/29700227/)
8. J. Debbache, V. Parfejevs, L. Sommer. Cre-driver lines used for genetic fate mapping of neural crest cells in the mouse: An overview. *Genesis* **56**, e23105 (2018). doi: [10.1002/dvg.23105](https://doi.org/10.1002/dvg.23105); pmid: [29673028](https://pubmed.ncbi.nlm.nih.gov/29673028/)
9. S. Picelli *et al.*, Full-length RNA-seq from single cells using Smart-seq2. *Nat. Protoc.* **9**, 171–181 (2014). doi: [10.1038/nprot.2014.006](https://doi.org/10.1038/nprot.2014.006); pmid: [24385147](https://pubmed.ncbi.nlm.nih.gov/24385147/)
10. A. Butler, P. Hoffman, P. Smibert, E. Papalexi, R. Satija. Integrating single-cell transcriptomic data across different conditions, technologies, and species. *Nat. Biotechnol.* **36**, 411–420 (2018). doi: [10.1038/nbt.4096](https://doi.org/10.1038/nbt.4096); pmid: [29680179](https://pubmed.ncbi.nlm.nih.gov/29680179/)
11. I. T. C. Ling, T. Sauka-Spengler. Early chromatin shaping pre-determines multipotent vagal neural crest into neural, neuronal and mesenchymal lineages. *Nat. Cell Biol.* **21**, 1504–1517 (2019). doi: [10.1038/s41556-019-0428-9](https://doi.org/10.1038/s41556-019-0428-9); pmid: [31792380](https://pubmed.ncbi.nlm.nih.gov/31792380/)
12. R. M. Williams *et al.*, Reconstruction of the global neural crest gene regulatory network in vivo. *Dev. Cell* **51**, 255–276.e7 (2019). doi: [10.1016/j.devcel.2019.10.003](https://doi.org/10.1016/j.devcel.2019.10.003); pmid: [31639368](https://pubmed.ncbi.nlm.nih.gov/31639368/)
13. W. Wurst, L. Bally-Cuif. Neural plate patterning: Upstream and downstream of the isthmus organizer. *Nat. Rev. Neurosci.* **2**, 99–108 (2001). doi: [10.1038/35053516](https://doi.org/10.1038/35053516); pmid: [11253000](https://pubmed.ncbi.nlm.nih.gov/11253000/)
14. D. Kobayashi *et al.*, Early subdivisions in the neural plate define distinct competence for inductive signals. *Development* **129**, 83–93 (2002). pmid: [11782403](https://pubmed.ncbi.nlm.nih.gov/11782403/)
15. M. Zervas, S. Millet, S. Ahn, A. L. Joyner. Cell behaviors and genetic lineages of the mesencephalon and rhombomere 1. *Neuron* **43**, 345–357 (2004). doi: [10.1016/j.neuron.2004.07.010](https://doi.org/10.1016/j.neuron.2004.07.010); pmid: [15294143](https://pubmed.ncbi.nlm.nih.gov/15294143/)

16. N. Hagan, M. Zervas, Wnt1 expression temporally allocates upper rhombic lip progenitors and defines their terminal cell fate in the cerebellum. *Mol. Cell. Neurosci.* **49**, 217–229 (2012). doi: [10.1016/j.mcn.2011.11.008](https://doi.org/10.1016/j.mcn.2011.11.008); pmid: [22173107](https://pubmed.ncbi.nlm.nih.gov/22173107/)
17. K. Takahashi, S. Yamanaka, Induction of pluripotent stem cells from mouse embryonic and adult fibroblast cultures by defined factors. *Cell* **126**, 663–676 (2006). doi: [10.1016/j.cell.2006.07.024](https://doi.org/10.1016/j.cell.2006.07.024); pmid: [16904174](https://pubmed.ncbi.nlm.nih.gov/16904174/)
18. A. Lignell, L. Kerosuo, S. J. Streichan, L. Cai, M. E. Bronner, Identification of a neural crest stem cell niche by Spatial Genomic Analysis. *Nat. Commun.* **8**, 1830 (2017). doi: [10.1038/s41467-017-01561-w](https://doi.org/10.1038/s41467-017-01561-w); pmid: [29184067](https://pubmed.ncbi.nlm.nih.gov/29184067/)
19. J. Kehler *et al.*, Oct4 is required for primordial germ cell survival. *EMBO Rep.* **5**, 1078–1083 (2004). doi: [10.1038/sj.embor.7400279](https://doi.org/10.1038/sj.embor.7400279); pmid: [15486564](https://pubmed.ncbi.nlm.nih.gov/15486564/)
20. H. R. Schöler, G. R. Dressler, R. Balling, H. Rohdewohld, P. Gruss, Oct-4: A germline-specific transcription factor mapping to the mouse t-complex. *EMBO J.* **9**, 2185–2195 (1990). doi: [10.1002/j.1460-2075.1990.tb07388.x](https://doi.org/10.1002/j.1460-2075.1990.tb07388.x); pmid: [2357966](https://pubmed.ncbi.nlm.nih.gov/2357966/)
21. K. M. Downs, Systematic localization of Oct-3/4 to the gastrulating mouse conceptus suggests manifold roles in mammalian development. *Dev. Dyn.* **237**, 464–475 (2008). doi: [10.1002/dvdy.21438](https://doi.org/10.1002/dvdy.21438); pmid: [18213575](https://pubmed.ncbi.nlm.nih.gov/18213575/)
22. R. Aires *et al.*, Oct4 is a key regulator of vertebrate trunk length diversity. *Dev. Cell* **38**, 262–274 (2016). doi: [10.1016/j.devcel.2016.06.021](https://doi.org/10.1016/j.devcel.2016.06.021); pmid: [27453501](https://pubmed.ncbi.nlm.nih.gov/27453501/)
23. C. Mulas *et al.*, Oct4 regulates the embryonic axis and coordinates exit from pluripotency and germ layer specification in the mouse embryo. *Development* **145**, dev159103 (2018). doi: [10.1242/dev.159103](https://doi.org/10.1242/dev.159103); pmid: [29915126](https://pubmed.ncbi.nlm.nih.gov/29915126/)
24. B. DeVeale *et al.*, Oct4 is required -E7.5 for proliferation in the primitive streak. *PLOS Genet.* **9**, e1003957 (2013). doi: [10.1371/journal.pgen.1003957](https://doi.org/10.1371/journal.pgen.1003957); pmid: [24244203](https://pubmed.ncbi.nlm.nih.gov/24244203/)
25. S. E. Creuzet, Regulation of pre-otic brain development by the cephalic neural crest. *Proc. Natl. Acad. Sci. U.S.A.* **106**, 15774–15779 (2009). doi: [10.1073/pnas.0906072106](https://doi.org/10.1073/pnas.0906072106); pmid: [19720987](https://pubmed.ncbi.nlm.nih.gov/19720987/)
26. D. H. Rowitch, A. P. McMahon, Pax-2 expression in the murine neural plate precedes and encompasses the expression domains of Wnt-1 and En-1. *Mech. Dev.* **52**, 3–8 (1995). doi: [10.1016/0925-4773\(95\)00380-J](https://doi.org/10.1016/0925-4773(95)00380-J); pmid: [7577673](https://pubmed.ncbi.nlm.nih.gov/7577673/)
27. S. Edri, P. Hayward, P. Baillie-Johnson, B. J. Steventon, A. Martinez Arias, An epiblast stem cell-derived multipotent progenitor population for axial extension. *Development* **146**, dev168187 (2019). doi: [10.1242/dev.168187](https://doi.org/10.1242/dev.168187); pmid: [31023877](https://pubmed.ncbi.nlm.nih.gov/31023877/)
28. H. Niwa *et al.*, Interaction between Oct3/4 and Cdx2 determines trophectoderm differentiation. *Cell* **123**, 917–929 (2005). doi: [10.1016/j.cell.2005.08.040](https://doi.org/10.1016/j.cell.2005.08.040); pmid: [16325584](https://pubmed.ncbi.nlm.nih.gov/16325584/)
29. Z. Simandi *et al.*, OCT4 Acts as an Integrator of Pluripotency and Signal-Induced Differentiation. *Mol. Cell* **63**, 647–661 (2016). doi: [10.1016/j.molcel.2016.06.039](https://doi.org/10.1016/j.molcel.2016.06.039); pmid: [27499297](https://pubmed.ncbi.nlm.nih.gov/27499297/)
30. C. Y. McLean *et al.*, GREAT improves functional interpretation of cis-regulatory regions. *Nat. Biotechnol.* **28**, 495–501 (2010). doi: [10.1038/nbt.1630](https://doi.org/10.1038/nbt.1630); pmid: [20436461](https://pubmed.ncbi.nlm.nih.gov/20436461/)
31. K. Aoto *et al.*, Mef2c-F10N enhancer driven β -galactosidase (LacZ) and Cre recombinase mice facilitate analyses of gene function and lineage fate in neural crest cells. *Dev. Biol.* **402**, 3–16 (2015). doi: [10.1016/j.ydbio.2015.02.022](https://doi.org/10.1016/j.ydbio.2015.02.022); pmid: [25794678](https://pubmed.ncbi.nlm.nih.gov/25794678/)
32. B. Pijuan-Sala *et al.*, Single-cell chromatin accessibility maps reveal regulatory programs driving early mouse organogenesis. *Nat. Cell Biol.* **22**, 487–497 (2020). doi: [10.1038/s41556-020-0489-9](https://doi.org/10.1038/s41556-020-0489-9); pmid: [32231307](https://pubmed.ncbi.nlm.nih.gov/32231307/)
33. R. Neijts *et al.*, Polarized regulatory landscape and Wnt responsiveness underlie Hox activation in embryos. *Genes Dev.* **30**, 1937–1942 (2016). doi: [10.1101/gad.285767.116](https://doi.org/10.1101/gad.285767.116); pmid: [27633012](https://pubmed.ncbi.nlm.nih.gov/27633012/)
34. K. M. Dorighi *et al.*, MII3 and MII4 facilitate enhancer RNA synthesis and transcription from promoters independently of H3K4 monomethylation. *Mol. Cell* **66**, 568–576.e4 (2017). doi: [10.1016/j.molcel.2017.04.018](https://doi.org/10.1016/j.molcel.2017.04.018); pmid: [28483418](https://pubmed.ncbi.nlm.nih.gov/28483418/)
35. V. Metzis *et al.*, Nervous system regionalization entails axial allocation before neural differentiation. *Cell* **175**, 1105–1118.e17 (2018). doi: [10.1016/j.cell.2018.09.040](https://doi.org/10.1016/j.cell.2018.09.040); pmid: [30343898](https://pubmed.ncbi.nlm.nih.gov/30343898/)
36. G. Couly, S. Creuzet, S. Bannaceur, C. Vincent, N. M. Le Douarin, Interactions between Hox-negative cephalic neural crest cells and the foregut endoderm in patterning the facial skeleton in the vertebrate head. *Development* **129**, 1061–1073 (2002). pmid: [11861488](https://pubmed.ncbi.nlm.nih.gov/11861488/)
37. M. Minoux *et al.*, Gene bivalency at Polycomb domains regulates cranial neural crest positional identity. *Science* **355**, eaal2913 (2017). doi: [10.1126/science.aal2913](https://doi.org/10.1126/science.aal2913); pmid: [28360266](https://pubmed.ncbi.nlm.nih.gov/28360266/)
38. P. Scerbo, A. H. Monsoro-Burq, The vertebrate-specific VENTX/NANOG gene empowers neural crest with ectomesenchyme potential. *Sci. Adv.* **6**, eaaz1469 (2020). doi: [10.1126/sciadv.aaz1469](https://doi.org/10.1126/sciadv.aaz1469); pmid: [32494672](https://pubmed.ncbi.nlm.nih.gov/32494672/)
39. A. Rada-Iglesias *et al.*, A unique chromatin signature uncovers early developmental enhancers in humans. *Nature* **470**, 279–283 (2011). doi: [10.1038/nature09692](https://doi.org/10.1038/nature09692); pmid: [21160473](https://pubmed.ncbi.nlm.nih.gov/21160473/)
40. A. Wang *et al.*, Epigenetic priming of enhancers predicts developmental competence of hESC-derived endodermal lineage intermediates. *Cell Stem Cell* **16**, 386–399 (2015). doi: [10.1016/j.stem.2015.02.013](https://doi.org/10.1016/j.stem.2015.02.013); pmid: [25842977](https://pubmed.ncbi.nlm.nih.gov/25842977/)
41. Y. Kojima *et al.*, The transcriptional and functional properties of mouse epiblast stem cells resemble the anterior primitive streak. *Cell Stem Cell* **14**, 107–120 (2014). doi: [10.1016/j.stem.2013.09.014](https://doi.org/10.1016/j.stem.2013.09.014); pmid: [24139757](https://pubmed.ncbi.nlm.nih.gov/24139757/)
42. C. Buecker *et al.*, Reorganization of enhancer patterns in transition from naive to primed pluripotency. *Cell Stem Cell* **14**, 838–853 (2014). doi: [10.1016/j.stem.2014.04.003](https://doi.org/10.1016/j.stem.2014.04.003); pmid: [24905168](https://pubmed.ncbi.nlm.nih.gov/24905168/)
43. S.-H. Yang *et al.*, ZIC3 controls the transition from naive to primed pluripotency. *Cell Rep.* **27**, 3215–3227.e6 (2019). doi: [10.1016/j.celrep.2019.05.026](https://doi.org/10.1016/j.celrep.2019.05.026); pmid: [31189106](https://pubmed.ncbi.nlm.nih.gov/31189106/)
44. M. R. Corces *et al.*, Lineage-specific and single-cell chromatin accessibility charts human hematopoiesis and leukemia evolution. *Nat. Genet.* **48**, 1193–1203 (2016). doi: [10.1038/ng.3646](https://doi.org/10.1038/ng.3646); pmid: [27526324](https://pubmed.ncbi.nlm.nih.gov/27526324/)
45. C. McQuin *et al.*, CellProfiler 3.0: Next-generation image processing for biology. *PLoS Biol.* **16**, e2005970 (2018). doi: [10.1371/journal.pbio.2005970](https://doi.org/10.1371/journal.pbio.2005970); pmid: [29969450](https://pubmed.ncbi.nlm.nih.gov/29969450/)

ACKNOWLEDGMENTS

We thank V. Ribes, K. Loh, S. Naqvi, and S. Kim for helpful comments on the manuscript and H. Nakauchi, E. Mizutani, and F. Suchy for generous help with animal experiments. **Funding:** This work was supported by the Howard Hughes Medical Institute, the National Institutes of Health (grant no. R35 GM131757), the Virginia and D.K. Ludwig Fund for Cancer Research (J.W.), EMBO (ALTF 275-2015), the European Commission (LTFCOFUND2013, GA-2013-609409), the Marie Curie Actions (A.Z.), the Polish National Science Center (ETIUDA 7 2019/32/T/NZ3/00370), and the University of Warsaw Integrated Development Programme (P.D.). **Author contributions:** A.Z., R.S., and J.W. conceived and designed the study. A.Z. and R.S. performed experiments with assistance from P.D. G.S.G. helped with single-cell RNA-seq processing and developmental trajectory analysis. D.J.W. optimized the ATAC-seq protocol. T.S. provided critical advice on experimental designs and performed data analyses. I.L.W. and J.W. supervised the project. A.Z., R.S., and J.W. wrote the manuscript with input from all authors. **Competing interests:** J.W. is a Camp4 SAB member. The remaining authors declare no competing interests. **Data and materials availability:** All data needed to evaluate the conclusions in this study are present in the main text, the supplementary materials, and/or the Gene Expression Omnibus (accession no. GSE162044).

SUPPLEMENTARY MATERIALS

science.sciencemag.org/content/371/6529/eabb4776/suppl/DC1
Materials and Methods
Figs. S1 to S20
Tables S1 to S3
References (46–56)
MDAR Reproducibility Checklist

[View/request a protocol for this paper from Bio-protocol.](#)

28 February 2020; accepted 20 November 2020
[10.1126/science.abb4776](https://doi.org/10.1126/science.abb4776)

Reactivation of the pluripotency program precedes formation of the cranial neural crest

Antoine Zalc, Rahul Sinha, Gunsagar S. Gulati, Daniel J. Wesche, Patrycja Daszczuk, Tomek Swigut, Irving L. Weissman and Joanna Wysocka

Science **371** (6529), eabb4776.
DOI: 10.1126/science.abb4776

Reactivating neural crest pluripotency

Cranial neural crest cells (CNCCs) are a transient cell group with an extraordinary differentiation potential that extends beyond its ectodermal lineage to form the majority of facial mesenchyme. Zalc *et al.* identified a neuroepithelial precursor population that transiently reactivates pluripotency factors to generate CNCCs. The pluripotency factor Oct4 is required for the expansion of CNCC developmental potential to form facial mesenchyme. Analysis of the chromatin landscape of Oct4⁺ CNCC precursors showed that these cells resemble those of epiblast stem cells, with additional features suggestive of future priming for neural crest programs. Thus, to expand their cellular potency, CNCC precursors undergo a natural in vivo reprogramming event.

Science, this issue p. eabb4776

ARTICLE TOOLS

<http://science.sciencemag.org/content/371/6529/eabb4776>

SUPPLEMENTARY MATERIALS

<http://science.sciencemag.org/content/suppl/2021/02/03/371.6529.eabb4776.DC1>

REFERENCES

This article cites 56 articles, 13 of which you can access for free
<http://science.sciencemag.org/content/371/6529/eabb4776#BIBL>

PERMISSIONS

<http://www.sciencemag.org/help/reprints-and-permissions>

Use of this article is subject to the [Terms of Service](#)

Science (print ISSN 0036-8075; online ISSN 1095-9203) is published by the American Association for the Advancement of Science, 1200 New York Avenue NW, Washington, DC 20005. The title *Science* is a registered trademark of AAAS.

Copyright © 2021 The Authors, some rights reserved; exclusive licensee American Association for the Advancement of Science. No claim to original U.S. Government Works